

# Evaluation of the ability of regional climate models and a statistical model to represent the spatial characteristics of extreme precipitation

Lichao Yang<sup>1</sup>  | Christian L. E. Franzke<sup>2,3</sup> | Zuntao Fu<sup>1</sup>

<sup>1</sup>Lab for Climate and Ocean-Atmosphere Studies, Department of Atmospheric and Oceanic Sciences, School of Physics, Peking University, Beijing, China

<sup>2</sup>Meteorological Institute, University of Hamburg, Hamburg, Germany

<sup>3</sup>Center for Earth System Research and Sustainability, University of Hamburg, Hamburg, Germany

## Correspondence

Zuntao Fu, Lab for Climate and Ocean-Atmosphere Studies, Department of Atmospheric and Oceanic Sciences, School of Physics, Peking University, Beijing, China.

Email: fuzt@pku.edu.cn

## Funding information

Deutsche Forschungsgemeinschaft, Grant/Award Number: 274762653; National Natural Science Foundation of China, Grant/Award Number: 41675049

## Abstract

Extreme precipitation is one of the most severe weather hazards which have a significant influence on society, agriculture and ecosystems. The spatial extension and intensity of extreme precipitation events are two important features which need to be quantified for improved flood risk and water resource management. Here, we evaluate how well regional climate models (RCMs) reproduce precipitation extremes with respect to spatial dependency and intensity. We show by using seasonal extreme intensities in Brandenburg-Berlin, Germany, that some RCMs underestimate the spatial dependence of extremes in summer and overestimate it in winter, compared with an observational-based data set. Most RCMs significantly underestimate the magnitudes of extremes in summer and overestimate the magnitudes in autumn and winter. A statistical model, based on a max-stable process, accounting for both the spatial and temporal variability is developed. We show that this model performs better in representing the spatial dependency and intensity characteristics of extreme precipitation compared to the RCMs.

## KEY WORDS

extreme precipitation, max-stable model, regional climate model, spatial extremes, spatial modelling

## 1 | INTRODUCTION

Precipitation is an important climatic variable and of socioeconomic importance. In particular, extreme precipitation is one of the most frequent and widespread severe weather hazards that may lead to flooding and landslides. Extreme precipitation events usually do not occur at a single location, but are spatially extended. As one would expect, there is a clear spatial correlation among extreme precipitation intensities at short to medium distances. This spatial dependence must be accurately reflected in statistical and regional climate models (RCMs) for risk assessments for hydrology, agriculture and insurance.

For instance, it is of utmost importance to accurately estimate the probability of joint, or spatial, extreme events. Consider three observations from the region we describe below: if spatial dependence is not considered, the probability that all three observations exceed their 50-year return level in the same year is 0.000008, which is severely underestimated and not realistic. In fact, a 50-year precipitation event which occurs simultaneously at those neighbouring locations has a much higher probability to occur of 0.01. Thus, it is crucial for risk management to accurately model the spatial dependence of extremes.

There are two main approaches to modelling extreme precipitation over a region. One is using RCMs, while the

other is using statistical models. RCMs, which resolve better the physical and dynamical processes than global climate models (GCMs), are able to represent precipitation at higher spatial and temporal resolutions. There are already many publications on evaluating the precipitation extremes of RCM output (Jones and Reid, 2001; Räisänen and Joellsson, 2001; Frei *et al.*, 2003; Bell *et al.*, 2004; Scherrer, 2011). It has been shown that the simulated heavy precipitation in RCMs have quite realistic magnitudes in central Europe (Räisänen and Joellsson, 2001; Ehmele *et al.*, 2019), but slightly underestimate observations in southern England and cannot well represent the seasonal extreme precipitation, defined by the high quantile of precipitation intensity over the European Alps (Jones and Reid, 2001; Frei *et al.*, 2003; Bell *et al.*, 2004). With the release of high spatial-temporal resolution RCM outputs, Sunyer *et al.* (2017) evaluated extreme precipitation of seven RCMs at different spatial and temporal aggregations over Denmark. They found, that the performance of the seven RCMs is similar for daily extreme precipitation intensity, but for hourly extreme precipitation the performance of RCMs differs. Several RCMs underestimate hourly precipitation intensities at short durations over Germany but overestimate them over Norway (Dyrrdal *et al.*, 2018; Berg *et al.*, 2019). Yang *et al.* (2019) also found that the RCMs fail to reproduce the power-law behaviour of hourly extreme rainfall.

However, most studies focus on evaluating the magnitude of the extremes, but are neglecting how RCMs reproduce the spatial dependence of the extremes. Since the RCM outputs are widely used to predict extreme events and act as important inputs for flood risk models, an accurate reproduction of the spatial dependence is essential when estimating the affected area and the probability of joint extreme events. Thus, the main aim of our study is to evaluate how the RCMs reproduce the spatial dependence of extreme precipitation.

Statistical precipitation models are constructed so that the computational expense of a high spatial resolution is minimized (e.g., Hannachi, 2014). For univariate extremes, the generalized extreme value (GEV) distribution is typically used to fit the maximum value in a fixed block, for example, annual maxima (Jenkinson, 1955). The probability distribution function of the GEV distribution is given by  $G(z) = \exp\left\{-[1 + \xi(\frac{z-\mu}{\sigma})]^{-\frac{1}{\xi}}\right\}$ , where  $\mu$ ,  $\sigma$  and  $\xi$  are the location, scale and shape parameters, respectively. When modelling extremes in a continuous space using statistical models, a simple method is the ‘spatial GEV’ model. The spatial GEV model means each GEV parameter is modelled independently by longitude and latitude of specific locations and potential covariates.

However, within the spatial GEV model, dependence between extremes is neglected. As we explained before, there will be a strong correlation between the extreme precipitation at relatively short distances, and this spatial dependence must be accurately included in any statistical model. For example, a 20-year precipitation event will not occur on a single point, but likely occurs also simultaneously at close by neighbouring locations. So the spatial dependence of extreme events must be included in statistical extreme models.

Recently, many statistical methods have been developed to model spatial dependency, such as latent variable models (Casson and Coles, 1999; Cooley *et al.*, 2007; Cooley and Sain, 2010), copulas (Bárdossy and Pegram, 2009; Bárdossy and Pegram, 2012) and max-stable random fields (Davison and Gholamrezaee, 2011; Thibaud *et al.*, 2013). The simplest approach to model spatial dependence is based on the Gaussian process with a variety of correlation functions  $\rho(h)$ , such as an exponential correlation function ( $\rho(h) = \exp(-\|h\|/\lambda)$ , where  $h$  is the distance). The latent variable models include the Gaussian process in each of the GEV parameters. For instance,  $\mu(x) = f_\mu(x; \beta_\mu) + S_\mu(x; \lambda_\mu)$ , where  $f_\mu(x; \beta_\mu)$  is a deterministic function depending on the regression parameters  $\beta_\mu$  like coordinates or covariates and  $S_\mu(x; \lambda_\mu)$  is a Gaussian process with unknown parameters  $\lambda_\mu$ . Similar formulations are also used in  $\sigma(x)$  and  $\xi(x)$ . This kind of spatial modelling has been applied in the extreme study of hurricane wind speeds (Casson and Coles, 1999) and precipitation (Cooley *et al.*, 2007; Cooley and Sain, 2010). However, the assumption that the Gaussian process for each GEV parameter is independent is not appropriate and leads to unrealistic spatial structures (Davison *et al.*, 2012).

The copula-based approach is intended to lead to a better spatial dependence modelling (Bárdossy and Pegram, 2009; Bárdossy and Pegram, 2012). The copula model is based on the assumption that one can represent the full probability density function (PDF) as the product of its marginal distributions and a copula, which encodes the spatial dependence structure (Schoelzel and Friederichs, 2008). Possible copulas are the Gaussian or Student-t copulas. However, some studies reported that the Gaussian copula model underestimates the spatial dependence and is far from being a universal tool for spatial modelling, especially for extremes (Renard and Lang, 2007; Davison *et al.*, 2012).

From a theoretical point of view, the generalization of classical multi-variate extreme-value distributions to a spatial model can be represented by a max-stable process (De Haan, 1984; De Haan and Pereira, 2006). Even though the theory of max-stable processes has been proposed over 20 years ago, the lack of a proper representation and

computational challenges have provided a barrier to further applications. Recently, pairwise likelihood fitting methods have been developed, paving the way of the theory into applications (Westra and Sisson, 2011; Ribatet, 2017).

In this study, we selected Brandenburg-Berlin, an important region for politics and agriculture in Germany, as our research region and aim to address the following research question: How well do RCMs and statistical models represent the extreme precipitation seen in historical observations with respect to spatial dependence and intensity? The format of the paper is as follows: In Section 2, we describe the study region, data set and max-stable model. In Section 3, we show the results of comparisons of RCMs and statistical models with observations. In Section 4 we conclude our study.

## 2 | DATA AND METHOD

### 2.1 | Study region

Brandenburg is located in the east of Germany, surrounding Berlin, the capital of Germany. About half of the area of Brandenburg is used for agricultural production. It has experienced repeatedly droughts and floods with serious damages in the past. The combination of low amounts of precipitation, high evaporation from lakes and low water storage capacity of the soil, can easily lead to drought conditions which directly influences agriculture and water supply in this area. However, more frequent extreme precipitation events will lead to more flooding events because of the soil structure in this area since the soil cannot take up the water quickly enough, likely leading to increased surface run off and floodings (Holsten *et al.*, 2009).

### 2.2 | Data

In order to study the spatial characteristics of extreme precipitation, we use the high-spatial resolution E-OBS data set. E-OBS is a  $0.1^{\circ}$  gridded daily precipitation data product. We use E-OBS version 18.0e during the time period January 1951 through December 2005. E-OBS 18.0e is an ensemble data set based on meteorological station measurements and is one of the highest spatial resolution data sets available. However, there are only 20 input stations in the study region. The interpolation method used to grid the station data were chosen after careful evaluation of a number of alternatives (Hofstra *et al.*, 2008). Another advantage of E-OBS is that it overcomes the scale mismatch between RCMs and observations (Hofstra *et al.*, 2010). Though satellite and radar can

provide high resolution and complete spatial coverage data, they have significant bias and only cover a short time period (New *et al.*, 2001; Gerstner and Heinemann, 2008). The observed data from meteorology stations show a mismatch of scale between accumulation and areal precipitation (Chen and Knutson, 2008). Compared with other gridded observation data sets, E-OBS is easily comparable with RCM outputs, as they share almost the same spatial resolution and time periods. Thus, the E-OBS data has been widely used in previous studies as an effective tool for model evaluation (Christensen *et al.*, 2010; Caroletti *et al.*, 2019).

To assess how RCMs reproduce the spatial-temporal characteristics of extreme precipitation, we use the following global and regional climate model combinations: CERFACS downscaled by CCLM4, MPI-ESM downscaled by CCLM4, HadGEM2 downscaled by RACMO22E, GFDL downscaled by REMO2015 and EC-EARTH downscaled by HIRHAM. The RCMs are collected by the Coordinated Regional Climate Downscaling Experiment program (CORDEX)(Jacob *et al.*, 2014) (<https://esgf-data.dkrz.de/search/cordex-dkrz/>). In order to compare with the observations within the same time period and spatial resolution, we select the historical simulations from 1951 to 2005 on grids of  $0.11^{\circ}$ . The extremes are defined by seasonal maxima (spring: MAM; summer: JJA; autumn: SON; winter: DJF).

### 2.3 | Max-stable process

The max-stable distribution (Ribatet, 2017) is described as follows: Let  $X_1, X_2, \dots$  be a sequence of independent copies of a random variable vector  $X$ . If there exist normalizing sequences  $\{c_n > 0: n \geq 1\}$  and  $\{d_n: n \geq 1\}$  such that

$$\frac{\max_{i=1,\dots,n} X_i - d_n}{c_n} \rightarrow Z, n \rightarrow \infty \quad (1)$$

in distribution, then provided it is nondegenerate, the random variable vector  $Z$  has a max-stable process. This description is based on the Fisher-Tippet-Gnedenko theorem (Coles *et al.*, 2001). For multiple locations, the marginal distribution of the variable  $Z$  are GEV distributed with different location, scale and shape parameters. Unlike spatial GEV models, the max-stable process permits spatial dependence.

The spatial dependence is characterized by the spectral representation of a max-stable process: Let  $Z(x): x \in \chi$  be a max-stable process with unit margins, that is, GEV  $(1,1,1)$  for all  $x \in \chi$  and  $z > 0$ , then

$$\{Z(x) : x \in \chi\} = \{\max_{i \geq 1} \xi_i Y_i(x) : x \in \chi\}, \quad (2)$$

where  $\{\xi_i : i \geq 1\}$  is a Poisson point process and  $\{Y_i(x) : x \in \chi\}$  is a sequence of independent copies of nonnegative stochastic processes  $\{Y_i(x) : x \in \chi\}$ . The  $Y_i(x)$  depicts the spatial dependence.

Based on the spectral representation of the max-stable process, we use four different models for  $\{Y_i(x) : x \in \chi\}$ , which are the Smith model, the Schlather model, the extremal- $t$  model and the Brown-Resnick model (Ribatet, 2017). Different models are likely to give different dependence structures. The specific expressions of the four models are listed in Table 1.  $\{\varepsilon(x), x \in \chi\}$  in the Schlather model is a standard Gaussian process with correlation function  $\rho(\cdot)$ , so that the Schlather model is also known as an extremal Gaussian model (Schlather, 2002). A generalization of this model is the extremal- $t$  model, which adds an exponent  $\nu$  (Davison *et al.*, 2012). Another widely used model is the Brown-Resnick model, where  $\{\varepsilon(x), x \in \chi\}$  is a Gaussian process with stationary increments and semi-variogram  $\gamma(\cdot)$ ,  $\gamma(h) = (h/\lambda)^\alpha$  (Brown and Resnick, 1977; Kabluchko *et al.*, 2009). The Smith model is a special case of the Brown-Resnick model with  $\alpha = 2$ .

According to the spectral representation of a max-stable process, there are two steps for modelling the extremes by statistical models: the first step is the modelling of the spatial dependence, and the second is the modelling of the marginal distributions. First we need to transfer each seasonal maximum series  $W$  to an unit-Frechet margin series  $Z$  by Equation (3) ( $\mu$ ,  $\sigma$  and  $\xi$  are location, scale and shape parameters of  $W$ ). Then we fit  $Z$  by either a Schlather, Smith, Extremal- $t$  and Brown-Resnick models using pairwise likelihood:

$$Z = \left[ 1 + \xi \frac{W - \mu}{\sigma} \right]^{\frac{1}{\xi}} \quad (3)$$

The fitting procedure is explained in detail by Ribatet (2009). To select the best model, we calculate the Takeuchi Information Criterion (TIC) value of each

**TABLE 1** Specific expressions of the spatial dependence models

Model	Expression
Schlather	$\{Y_i(x) : x \in \chi\} = \sqrt{2\pi} \max\{0, \varepsilon(x)\} : x \in \chi$
Extremal- $t$	$\{Y_i(x) : x \in \chi\} = \{c_\nu \max\{0, \varepsilon(x)\}^\nu : x \in \chi\}$ , $c_\nu = \sqrt{\pi} 2^{-\frac{\nu-2}{2}} \Gamma\left(\frac{\nu+1}{2}\right)$
Brown- Resnick	$\{Y_i(x) : x \in \chi\} = \{\exp\{\varepsilon(x) - \gamma(x)\}, x \in \chi\}$ , $\gamma(x) = (x/\lambda)^\alpha$
Smith	$\{Y_i(x) : x \in \chi\} = \{\exp\{\varepsilon(x) - \gamma(x)\}, x \in \chi\}$ , $\gamma(x) = (x/\lambda)^2$

model. TIC is equivalent to the Akaike Information Criterion (AIC) when the model is miss-specified (Burnhan and Anderson, 2002; Varin and Vidoni, 2005). The model with minimum TIC value can be considered to be the optimal one. The second step is the marginal distribution modelling. The marginal distributions of maximum precipitation are modelled by a GEV distribution with grid point dependent location, scale and shape parameters and temporal covariats. The maximum-likelihood method is used for the estimating of the parameters of the GEV distribution and the optimal model is chosen by TIC values as well. After we have chosen the best spatial and marginal models, we will use the inverse function of Equation (3) to combine them.

## 2.4 | Spatial dependence coefficient

To quantify the spatial dependence between grid points, a common tool in geo-statistics is the madogram (Cooley *et al.*, 2006). Here, we use the extremal coefficient to estimate the spatial dependence coefficient based on the F-madogram proposed by Cooley *et al.* (2006). The F-madogram is defined as follows,

$$\nu_F(x_1 - x_2) = \frac{1}{2} E[F(Z(x_1)) - F(Z(x_2))], \quad (4)$$

where  $F(z) = \exp(-1/z)$  is a stationary max-stable random field with unit-Frechet margins. More precisely, we first extract series of seasonal maxima ( $W(x)$ ) on each grid point and transform them to series with unit-Frechet margins ( $Z(x)$ ) by Equation (3).

Then we apply Equation (5) to each pair of grid points,

$$\nu_F(x_1 - x_2) = \frac{1}{2n} \sum_{i=1}^n |F(z_i(x_1)) - F(z_i(x_2))| \quad (5)$$

where  $z_i(x_1)$  and  $z_i(x_2)$  are the  $i$ -th observations of  $Z(x)$  at locations  $x_1$  and  $x_2$  and  $n$  is the total number of observations. The extremal coefficient has a one-to-one relation with the F-madogram and is defined by,

$$\theta(x_1 - x_2) = \frac{1 + 2\nu_F(x_1 - x_2)}{1 - 2\nu_F(x_1 - x_2)}. \quad (6)$$

$\theta$  is the extremal coefficient and lies between 1 and 2. When  $\theta = 1$  the two observations are totally dependent and for  $\theta = 2$  the two observations are independent.

Another estimator is called the extremal concurrence coefficient which is proposed by Dombry *et al.* (2018).

While it is also an estimator of spatial dependence, it is intended to quantify the probability of extremal concurrence. The extremal concurrence coefficient is defined by

$$p(s_1, \dots, s_k) = P\{\text{for some } l \geq 1 : \eta(s_j) = \varphi_l(s_j), j=1, \dots, k\} \quad (7)$$

It has been proved that when  $k = 2$ , pairwise extremal concurrence probability for max-stable vectors is precisely equal to Kendall's  $\tau$  (Dombry *et al.*, 2018). For any max-stable process  $\eta$ , the extremal concurrence probability  $p(s_1, s_2)$  can be calculated as follows

$$\begin{aligned} p(s_1, s_2) &= \tau_{\eta(s_1), \eta(s_2)} \equiv E[\text{sign}\{\eta(s_1) - \eta_*(s_1)\} \text{sign}\{\eta(s_2) \\ &\quad - \eta_*(s_2)\}] \end{aligned} \quad (8)$$

where  $\eta_*$  is an independent copy of  $\eta$ . The range of  $p(s_1, s_2)$  ranges from 0 to 1. For  $p(s_1, s_2) = 0$   $\eta(s_1)$  and  $\eta(s_2)$  are independent and for  $p(s_1, s_2) = 1$   $\eta(s_1)$  and  $\eta(s_2)$  are totally dependent.

### 3 | RESULTS

#### 3.1 | Extreme precipitation simulated by RCMs

##### 3.1.1 | Evaluation of spatial dependence of extremes

In the Brandenburg-Berlin region, the highest frequency of extreme precipitation occurs in summer. It is therefore natural to have a special focus on the summer season.

To better understand the concept of spatial dependence, we first choose one base point  $s_0$  (Potsdam, 12.95 E, 52.95 N) and compute the extremal concurrence coefficient over all pairs of grid points  $(s_0, s)$ . This allows us to quantify how fast the spatial dependence between precipitation extremes decreases when moving away from  $s_0$ . Figure 1 shows the position of the selected base point and the spatial distributions of the interpolated extremal concurrence coefficient for the summer during 1951 to 2005 for both observations and RCMs. As

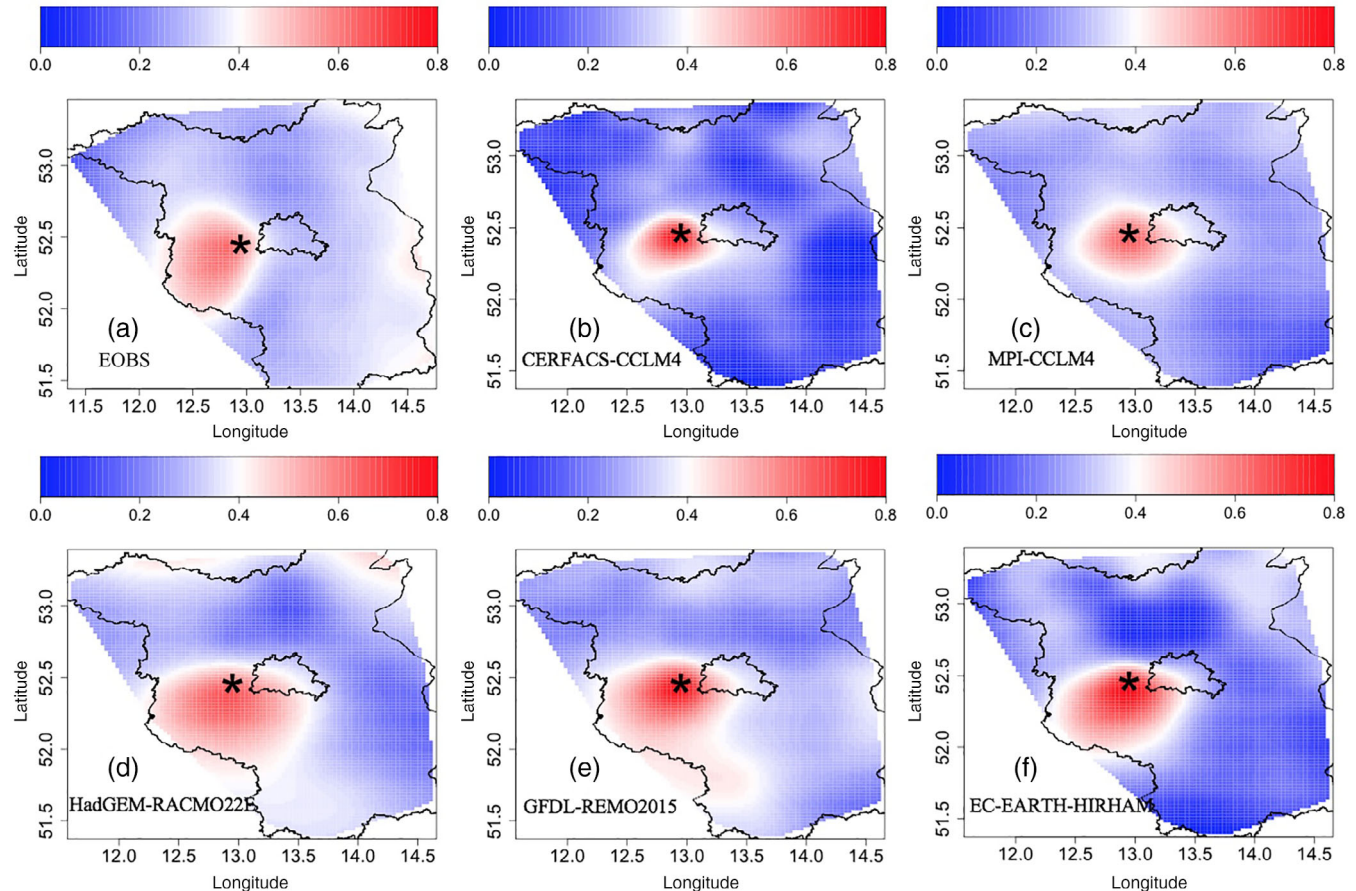


**FIGURE 1** Maps of extremal concurrence coefficient computed between the base grid point at 12.95 E, 52.95 N and all other grid points for (a) observations and (b) CERFACS-CCLM4, (c) MPI-CCLM4, (d) HadGEM-RACMO22E, (e) GFDL-REMO2015, (f) EC-EARTH-HIRHAM regional climate models in summer. The base grid point is marked by star [Colour figure can be viewed at [wileyonlinelibrary.com](http://wileyonlinelibrary.com)]

expected, the highest dependence occurs in the neighbourhood of the base point. When the grid points move away from  $s_0$ , the dependence weakens. The amount of weakening is asymmetric and decreases much faster to the east than the west, which means that the extremes of  $s_0$  have a larger impact on the region to their west. The extremes in the west of the base point are more likely to be affected. When we selected different base points  $s_0$ , this west–east asymmetry always exists, making

this a robust feature. Even for Berlin, where the input station network is denser than in other regions, the west–east asymmetry exists as well. So the varying input station density of E-OBS does not have a big effect on the observed east–west asymmetry. A possible explanation is that most rainfall systems come from the west, so that most precipitation will fall at or behind the front but less in front of the front (in the east). Then extreme precipitation in the western areas are more likely to occur

**TABLE 2** Average and SD values of extremal concurrent coefficients ( $p$ ) between other grids and the selected grid  $s_0$ .

	E-OBS	C-CCL4	MPI-CCL4	Had-RAC
Summer	<b>0.33 (0.08)</b>	0.19 (0.12)	0.28 (0.09)	0.33 (0.11)
Winter	<b>0.39 (0.06)</b>	0.42 (0.09)	0.50 (0.11)	0.49 (0.11)
	GFDL-REM	EC-HIR	<b>Max-stable</b>	
Summer	0.32 (0.11)	0.25 (0.14)	<b>0.34 (0.09)</b>	
Winter	0.46 (0.09)	0.32 (0.13)	<b>0.36 (0.08)</b>	

Note: C-CCL4 is short for CERFACS-CCLM4; MPI-CCL4 is short for MPI-CCLM4; Had-RAC is short for HadGEM-RACMO22E; GFDL-REM is short for GFDL-REMO2015; EC-HIR is short for EC-EARTH-HIRHAM.

The results of E-OBS and Max-stable model are marked in bold.

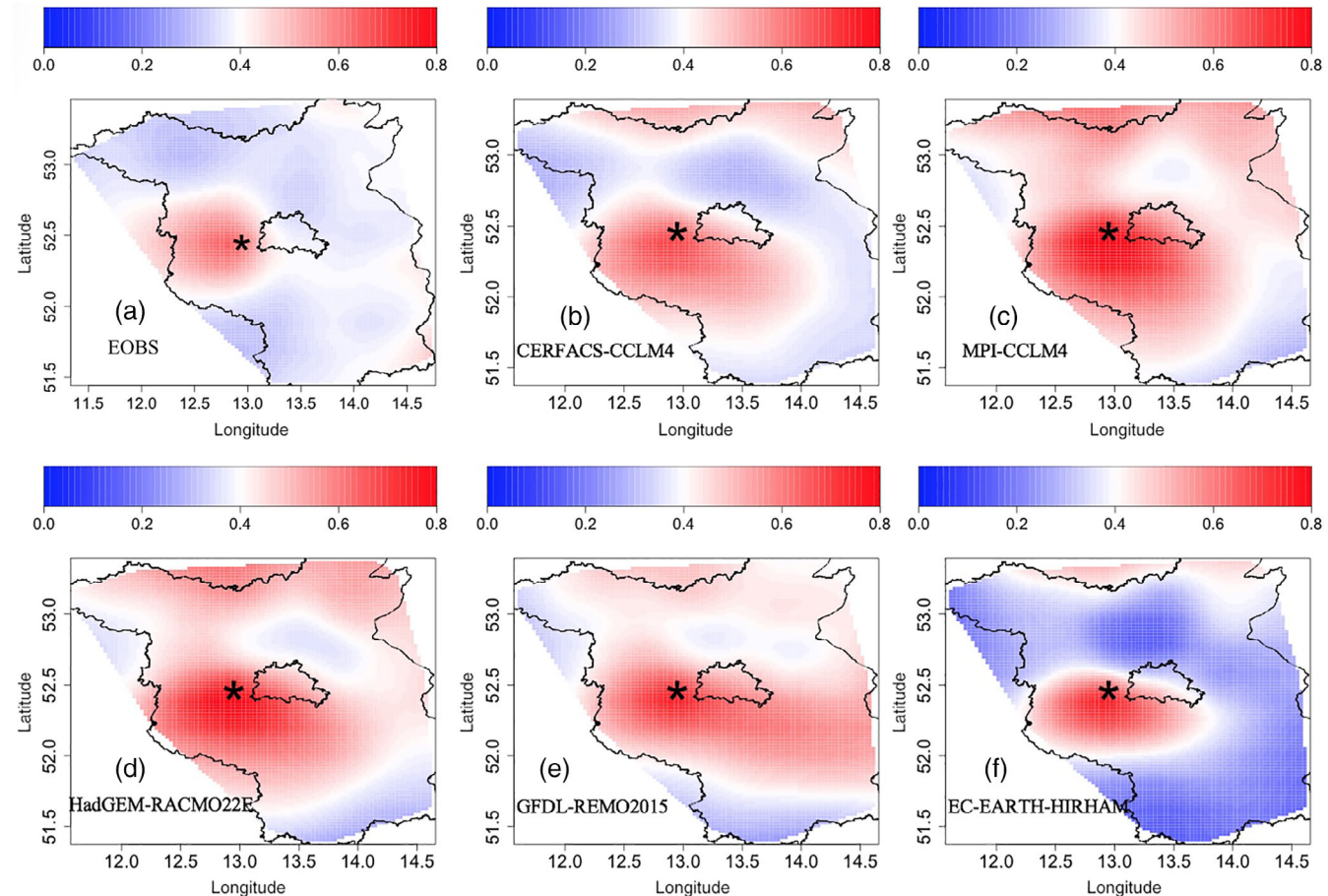


**FIGURE 2** Same as Figure 1 but for winter [Colour figure can be viewed at [wileyonlinelibrary.com](http://wileyonlinelibrary.com)]

simultaneously with the base point. The extremes in the RCMs show similar patterns as E-OBS. They are able to show that the dependence weakens when the grid is far away from  $s_0$ . The average and  $SD$  values of  $p$  are shown in Table 2. In CERFACS-CCLM4 and EC-REMO2015, the dependence in most grids is underestimated. So the mean values of  $p$  in these two RCMs are much smaller than E-OBS. Other RCMs show similar mean values as the observations. However, none of the RCMs show the observed west–east asymmetric feature visible in E-OBS. In particular, in CERFACS-CCLM4 and MPI-CCLM4,  $p$  weakens uniformly away from  $s_0$ . The dependencies in the southern parts are overestimated by HadGEM-RACMO22E, GFDL-REMO2015 and EC-EARTH-HIRHAM.

In winter, the spatial dependence of extremes becomes stronger (Figure 2 and Table 2). Compared with the results of E-OBS in summer, the  $p$  values at most grids increase, which means the dependence of extremes in winter becomes stronger ( $\bar{p}_{\text{summer}} = 0.33 \pm 0.08$ ,  $\bar{p}_{\text{winter}} = 0.39 \pm 0.06$ ). It may be due to that most of the extreme precipitation events in summer are caused by convective systems, which are

more localized. While extreme precipitation events in winter are more likely caused by large-scale precipitation so that the extremes over larger areas are more strongly correlated. Similar results are also obtained from Cabrals' paper, in which they evaluated the spatial homogeneity over the North-Western Germany and found the spatial dependence during winter is stronger than during summer (Cabral *et al.*, 2019). The asymmetric decay of dependence between the western and eastern parts of the selected grid points also exists in winter. The ability of RCMs in reproducing the spatial dependence between other grid points and  $s_0$  (Potsdam, 12.95 E, 52.95 N) in winter is even worse. The RCMs are able to show the stronger spatial dependence (Table 2), but all of the RCMs show an overestimation of the size of high spatial dependence area, especially CERFACS-CCLM4, MPI-CCLM4, HadGEM-RACMO22E and GFDL-REMO2015, while EC-EARTH-HIRHAM shows an underestimation of the spatial dependence when the grid points are far away from  $s_0$ , but an overestimation when the grid points are close to  $s_0$ . Besides, none of the RCMs are able to reproduce the west–east

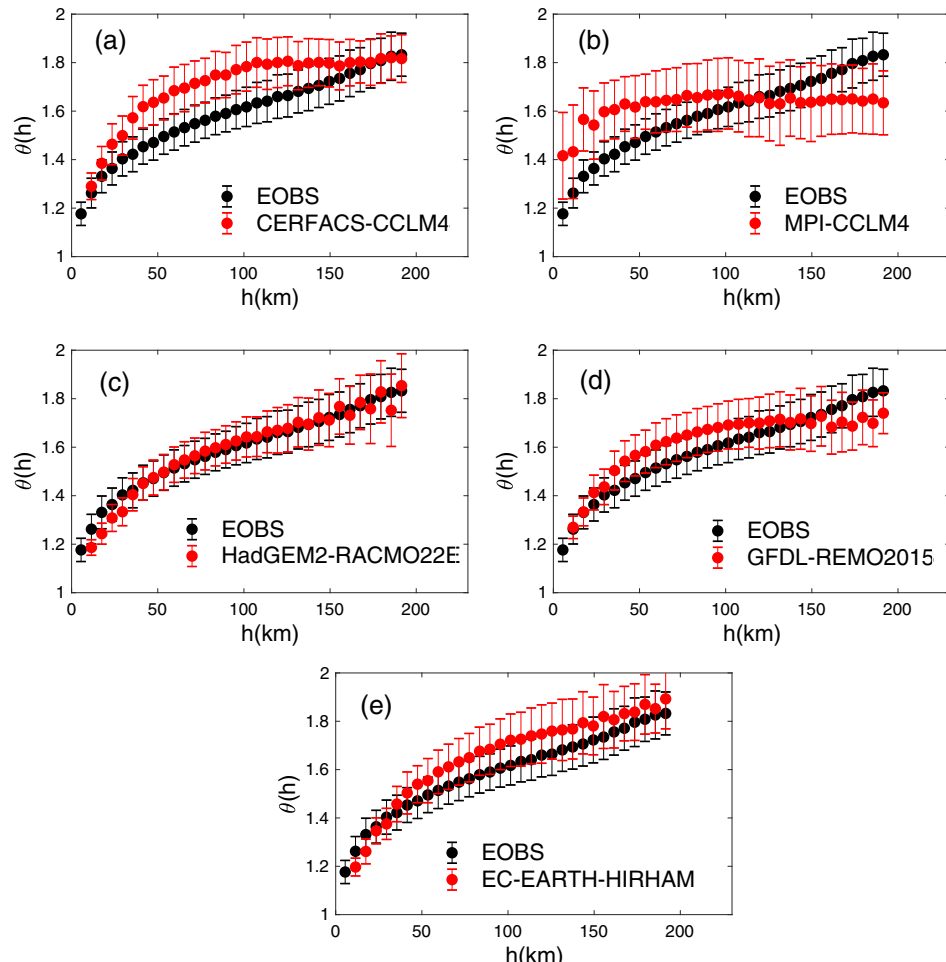


**FIGURE 3** Probability distribution of pairwise extremal coefficients between observation (black circles) and regional climate model outputs (red circles) in summer. Error bars correspond to one  $SD$  [Colour figure can be viewed at [wileyonlinelibrary.com](http://wileyonlinelibrary.com)]

asymmetry of the decay of dependence. Thus, the RCMs have shortcomings in modelling the specific spatial dependence of extreme precipitation in summer and winter. The reason why the RCMs cannot well reproduce the real pattern may be caused by the deficiencies in modelling the large-scale rainfall systems. However, this needs further research which is beyond the scope of the present study.

Although Figures 1 and 2 show how the other grid points are affected by extreme events occurring at  $s_0$ , it has the drawback of being dependent on the selected particular location. To show the spatial dependence over the whole region, we compute the probability distribution of the extremal coefficient ( $\theta$ ) over all pairs of grid points. Figure 3 compares the probability distribution and uncertainties of  $\theta$  of observations and RCMs in summer. As the distance between two grid points increases, the dependence weakens. On the range of 50 to 200 km, the relationship between  $\theta(h)$  and  $h$  of observation is almost a linear one. Even when two grid points are 200 km apart, the extremes are still significantly dependent on each other. Consistent with Figure 1, the combinations of CERFACS-CCLM4, GFDL-REM2015 and EC-EARTH-

HIRHAM models all underestimate the spatial dependence to some extent. CERFACS-CCLM4 significantly underestimates the spatial dependence when the distance ranges from 40 to 110 km. When the distance reaches 120 km, the mean value of  $\theta$  does not change with distance any longer. The mean value of the extremal coefficient of the MPI-CCLM4 model does not change much with distance over the whole range that leads to a significant underestimation of the dependence when the distance is shorter than 40 km and an overestimation when the distance is around 200 km. This effect may be related to the weak spatial dependence of convective precipitation and the spatially more homogeneous large-scale precipitation. We have also examined the convective precipitation output and compare this with the total precipitation amounts of the MPI-CCLM4 model. It shows that the short-range dependence is mostly due to the convective precipitation, while the long-range is affected by large-scale precipitation. It indicates that the MPI-CCLM4 lacks the ability to describe the spatial variability of extremes in this region and improvements of subgrid and large-scale parameterization schemes are needed (Rulfová *et al.*, 2017). GFDL-REMO2015 and EC-EARTH-

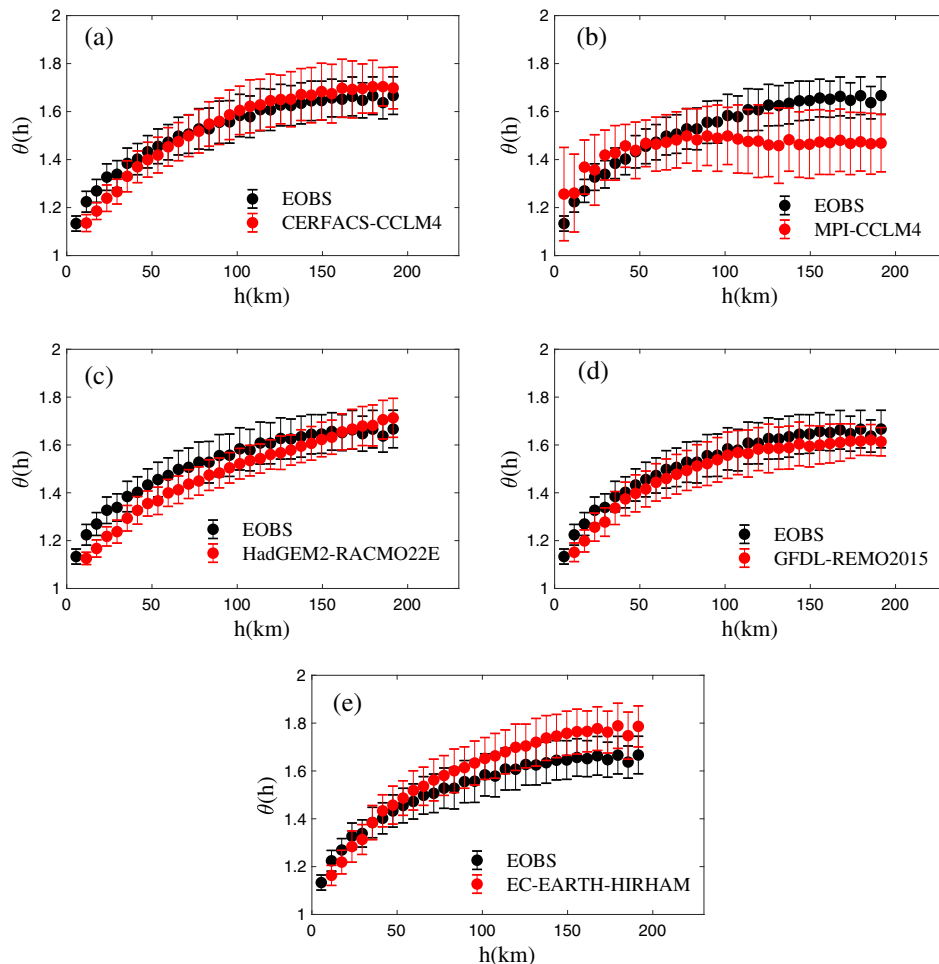


**FIGURE 4** Same as Figure 3 but for winter [Colour figure can be viewed at [wileyonlinelibrary.com](http://wileyonlinelibrary.com)]

HIRHAM show an insignificant underestimation when the distance is longer than 50 km. HadGEM2-RACMO22E behaves the best in characterizing the dependence of extremes. Both the mean value and the uncertainties of extremal coefficient are overlapping well with observations.

In winter, none of the probability distributions of extremal coefficients for the RCMs overlap exactly with the observations (Figure 4). However, for most RCMs these deviations are not significant. For most RCMs the observations are inside the uncertainty bound, as measured by one  $SD$ , of the RCM estimates. It is noteworthy, that for MPI-CCLM4 mean value of the extremal coefficients does not change with the distance. For many distances this deviation is significant. This may be a general problem of MPI-CCLM4 in reproducing the spatial dependence of extremes, and is not dependent on the season. GFDL-REMO2015 in spring and CERFACS-CCLM4 in autumn can well reproduce the spatial dependence of extremes compared with the observations (not shown).

### 3.1.2 | Evaluation of the magnitudes of extremes

With the extremal concurrent coefficient ( $p$ ) and extremal coefficient ( $\theta$ ), we can estimate how one single

extreme event affects the area surrounding it. It also provides us with a novel way to evaluate the ability of RCMs to reproduce realistic precipitation extreme events. Besides the spatial dependence of extremes, how well RCMs reproduce the intensities is another important research question. In hydrology studies, return levels and return periods are widely used to describe and quantify risk of extremes, so we first take the 50-year return level distribution as an example. The return level is estimated by maximum likelihood and the uncertainties are based on the delta method (Coles *et al.*, 2001).

Figure 5 compares the distribution of the 50-year return value of 1-day precipitation extremes ( $x_{1d.50}$ ) between E-OBS and the RCMs in summer. For E-OBS, large values of  $x_{1d.50}$  are observed at some grid points in the north-eastern part of Brandenburg. There is a big difference between the values in the south-east and north-west. The values in the south-east are mostly larger than in the north-west. Most of the values in the north-western part are below 80 mm, while most values in the south-east are between 80 and 100 mm. Among the RCMs, CERFACS-CCLM4 and MPI-CCLM4 do not show many spatial differences over the whole region, which is consistent with our analysis of the spatial dependence. They lack the ability to characterize the spatial dependence of the extremes and severely underestimate the

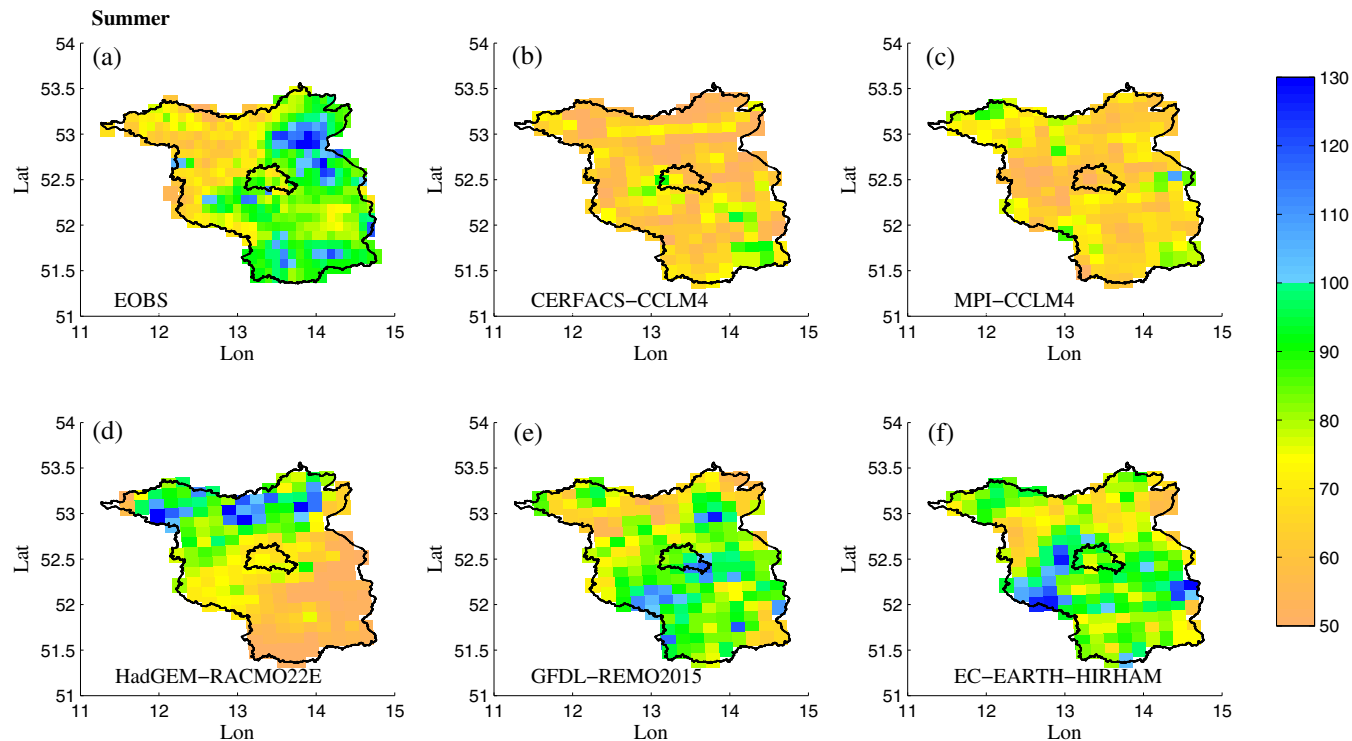


**FIGURE 5** Maps of return levels in mm at 50-year return periods from (a) observation and (b) CERFACS-CCLM4, (c) MPI-CCLM4, (d) HadGEM-RACMO22E, (e) GFDLREMO2015, (f) EC-EARTH-HIRHAM regional climate models in summer [Colour figure can be viewed at [wileyonlinelibrary.com](http://wileyonlinelibrary.com)]

return values. HadGEM2-RACMO22E shows the best spatial dependence (Figure 3), however, it shows the opposite spatial distribution of intensities of extremes, in

**TABLE 3** Mean  $\Delta$  values (%) between different RCMs and observation in summer and winter; 5 and 95% confidence intervals shown in brackets

	C-CCL4	MPI-CCL4	Had-RAC
Summer	24.38 (13.41, 35.35)	23.27 (12.96, 33.58)	30.83 (20.52, 41.14)
Winter	10.14 (5.71, 14.57)	7.73(6.46, 9)	13.38 (8.38, 18.38)
	GFDL-REM	EC-HIR	
Summer	16.45 (13.98, 18.92)	21.05 (17.35, 24.75)	
Winter	22.48 (19.68, 25.28)	20.06 (12.87, 27.25)	

which large values are located in the north-west. The GFDL-REMO2015 and EC-EARTH-HIRHAM models show some differences of return values between the northern and southern part. However, they are not good enough to present the differences between the north-west and south-east. To quantify the differences at each location, we select the closest grid point of RCM to compare with observation grid and compute the mean deviation from the observations (Equation (9)) (Table 3). It reveals that GFDL-REMO2015 reproduces the magnitudes best in summer ( $\Delta = 16.45\%$ ) and MPI-CCLM4 is best in winter ( $\Delta = 7.73\%$ ).

$$\Delta = \frac{1}{n} \sum_{i=1}^n \frac{|x_{i,RCM} - x_{i,OBS}|}{x_{i,OBS}} \times 100\% \quad (9)$$

The extreme magnitudes for other return levels are shown by quantile plots. The quantile plots of maximum

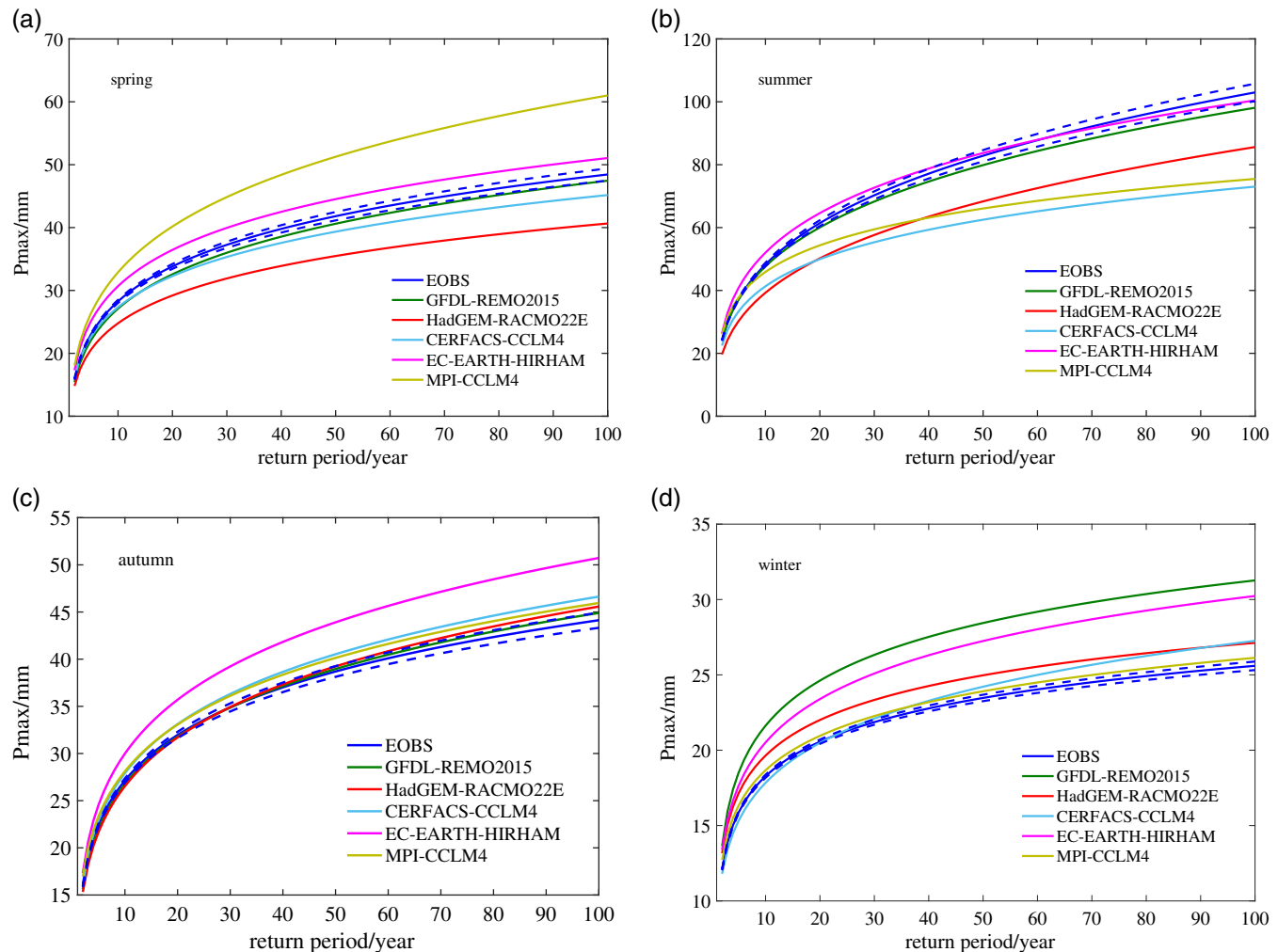


**FIGURE 6** Quantile plots of the extreme precipitation in each season of EOBS and five regional climate model output. The quantile are calculated by all the study grid boxes. The dashed lines are 5 and 95% confidence limits of EOBS [Colour figure can be viewed at [wileyonlinelibrary.com](http://wileyonlinelibrary.com)]

precipitation in each season of the five RCMs and observations are presented in Figure 6. It shows the estimates of maximum precipitation as a function of return period. In the spring season, the extremes from MPI-CCLM4 and EC-EARTH-HIRHAM are significantly overestimated and the CERFACS-CCLM4 and HadGEM-RACMO22E are significantly underestimated (the confidence intervals of RCMs are not shown). GFDL-REMO2015 is the best in estimating the magnitude of maximum precipitation. It is very close to the results of the E-OBS observations. Similar with the results we mentioned before, in summer, MPI-CCLM4, HadGEM-RACMO22E and CERFACS-CCLM4 show a significant underestimation when the return period is longer than 10 years. GFDL-REMO2015 and EC-EARTH-HIRHAM estimate the extremes quite well, almost overlapping with the observations. In autumn, the extremes are overestimated by the RCMs. Among them, the EC-EARTH-HIRHAM and CERFACS-CCLM4 show a significant overestimation. In winter, the RCMs still show an overestimation. The values of MPI-CCLM4 are the closest to the E-OBS observations. The other four RCMs, especially GFDL-REMO2015, EC-EARTH-HIRHAM and HadGEM-RACMO22E show also significant overestimation.

In summary, we evaluated how well five RCMs can simulate extreme precipitation with respect to spatial dependence and intensity over Brandenburg-Berlin. The CERFACS-CCLM4 and MPI-CCLM4 models lack the ability to characterize both the spatial dependencies and the intensities in summer. HadGEM-RACMO22E shows similar magnitudes but opposite spatial distributions. GFDL-REMO2015 and EC-EARTH-HIRHAM underestimate both the spatial dependence and the intensities. The quantile plots between the RCMs and observations show that some RCMs significantly underestimate the magnitudes of extremes in summer and overestimate

them in autumn and winter. Some RCMs have biases up to dozens of percent.

### 3.2 | Extreme precipitation simulated by a statistical model

#### 3.2.1 | Spatial dependence modelling

The spatial dependence of extreme precipitation events of observations is modelled first. Figure 7 shows the comparison of the extremal coefficients between E-OBS and the fitted max-stable models in summer and winter. Apart from the Smith model, the others behave well in characterizing the spatial dependence of extreme precipitation. The Smith model overestimates the dependence at short distances and severely underestimates it at long distances. It reaches independence at about 150 km, which occurs much earlier compared to E-OBS. The goodness of fit is quantified by TIC values. Table 4 shows the TICs of different models. The Smith model has the maximum TIC values and the Extremal-*t* model has the minimum. So we adopt the Extremal-*t* model for the spatial dependence modelling.

**TABLE 4** TIC values of different models

Model	TIC (summer)	TIC (winter)
Schlather	44,496,553	44,084,832
Smith	45,005,345	44,573,310
<b>Extremal-<i>t</i></b>	<b>44,363,579</b>	<b>43,915,408</b>
Brown-Resnick	44,389,460	43,967,066

Note: The best model is marked in bold.

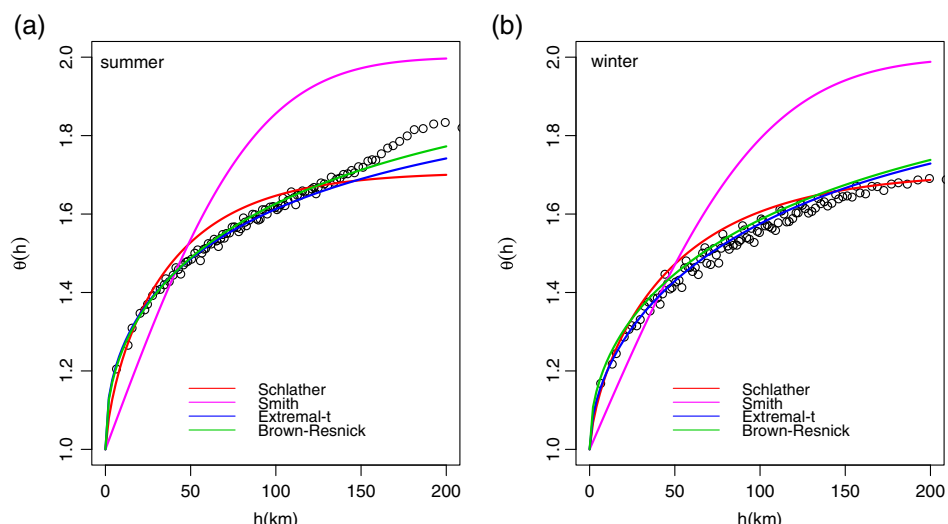


**FIGURE 7** The extremal coefficient between observation (circles) and the fitted max-stable model (lines) in (a) summer and (b) winter [Colour figure can be viewed at [wileyonlinelibrary.com](http://wileyonlinelibrary.com)]

### 3.2.2 | Marginal distribution modelling

The marginal distributions of maximum precipitation are modelled by a GEV distribution with grid point dependent location, scale and shape parameters. Specifically, the location, scale and shape parameters are modelled spatially as a function of longitude and latitude over the region. We also include mean surface air temperature averaged over

this region ( $T$ ) and the North Atlantic Oscillation (NAO) index as temporal covariates (like Equation (10))

$$\begin{aligned}\mu(x, T, NAO) &= \beta_0 + \beta_1 \text{lon}(x) + \beta_2 \text{lat}(x) + \beta_3 T + \beta_4 \text{NAO} \\ \sigma(x, T, NAO) &= \beta_0^1 + \beta_1^1 \text{lon}(x) + \beta_2^1 \text{lat}(x) + \beta_3^1 T + \beta_4^1 \text{NAO} \\ \xi(x, T, NAO) &= \beta_0^2 + \beta_1^2 \text{lon}(x) + \beta_2^2 \text{lat}(x) + \beta_3^2 T + \beta_4^2 \text{NAO}\end{aligned}\quad (10)$$

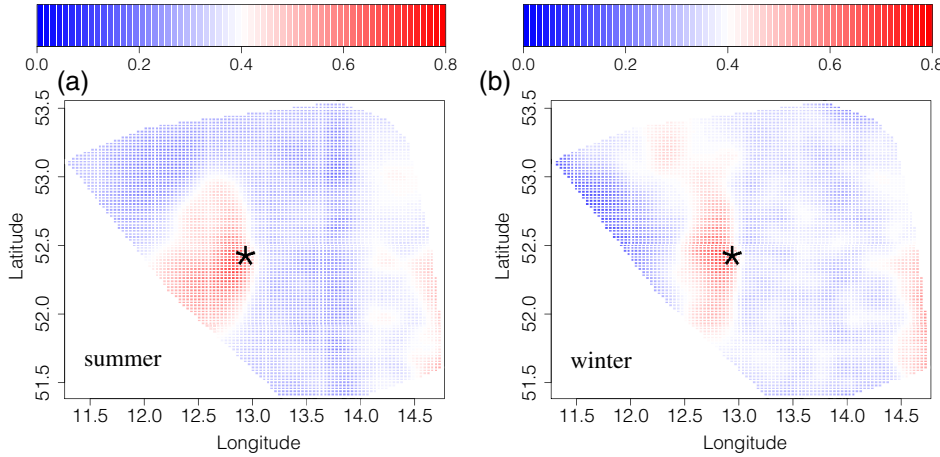


**FIGURE 8** Maps of extremal concurrence coefficient computed between the base grid point at 12.95 E, 52.95 N and all other grid points for observations and the max-stable model in (a) summer and (b) winter. The base grid point is marked by star [Colour figure can be viewed at [wileyonlinelibrary.com](http://wileyonlinelibrary.com)]

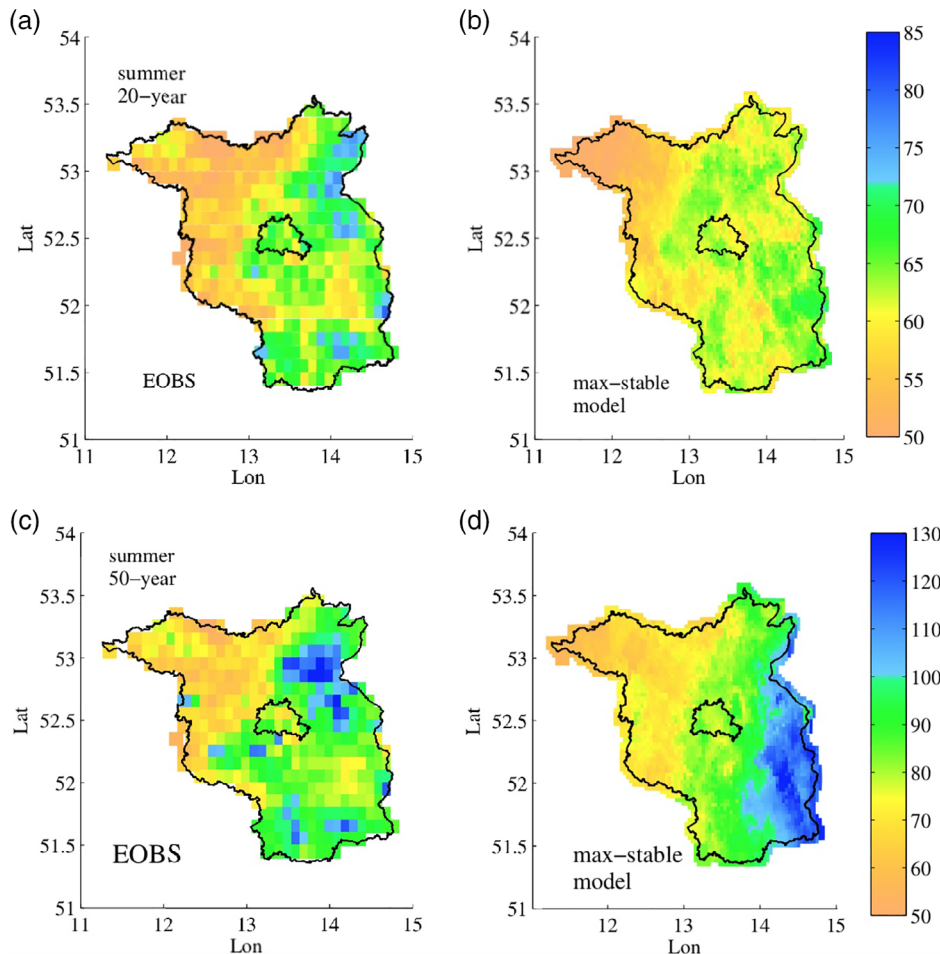
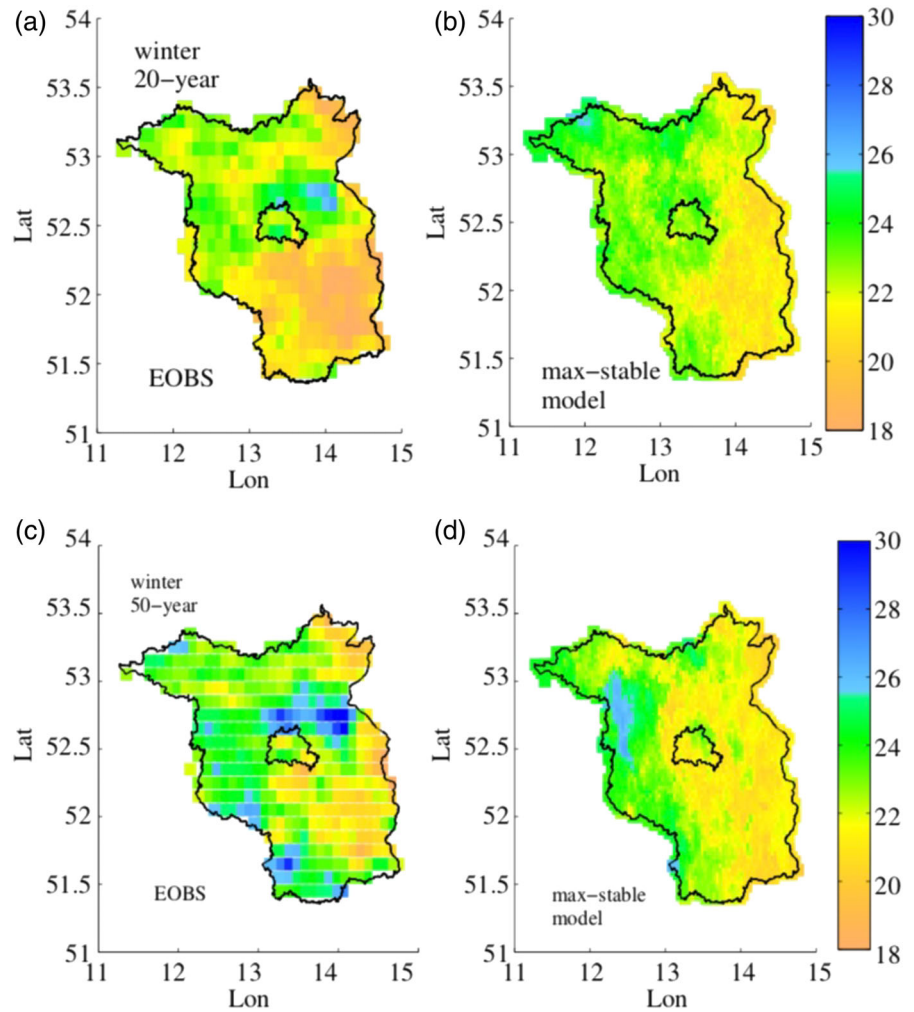


**FIGURE 9** Maps of return levels in mm at 20- and 50-year return periods from (a,c) observation and (b,d) the max-stable model in summer [Colour figure can be viewed at [wileyonlinelibrary.com](http://wileyonlinelibrary.com)]

**FIGURE 10** Same as Figure 9 but for winter [Colour figure can be viewed at [wileyonlinelibrary.com](http://wileyonlinelibrary.com)]



According to Equation (10), each parameter has  $2^4 = 16$  combinations and there are  $16^3 = 4,096$  combinations in total ( $\beta_0, \beta_0^1, \beta_0^2$  must be included). We fit the E-OBS extreme precipitation at each grid point to a GEV distribution for each parameter combination, estimate  $\beta$  using maximum-likelihood, calculate each TIC value and finally select the model with the minimum TIC value. When we compute all the TIC values of the combinations, we find the following model gets the smallest TIC value. In summer, the model without any covariate has the smallest TIC value (Equation (11))

$$\begin{aligned} & \tilde{\mu}_{lat} \\ & \tilde{\sigma}_{lon} \\ & \tilde{\xi}_{lon} \end{aligned} \quad (11)$$

while in winter, there is a large reduction in TIC when including the temperature as a covariate, indicating that global warming has an influence on the

extreme precipitation in winter but not in summer (Equation (12))

$$\begin{aligned} & \tilde{\mu}_{lat} + lon + T \\ & \tilde{\sigma}_{lon} \\ & \tilde{\xi}_1 \end{aligned} \quad (12)$$

This is consistent with Moberg *et al.* (2006) and Scherrer *et al.* (2016) research that the extreme intensities in winter are increasing significantly, but the extreme intensities in summer show no overall trend. The NAO also plays an important role for the precipitation extremes intensity in winter (Santos *et al.*, 2007; Casanueva Vicente *et al.*, 2014). As stated by Santos and his co-authors, the NAO is the leading large-scale circulation mode which affects the occurrence of winter heavy precipitation. When we include the NAO as a temporal covariate in the marginal model, the TIC reduces when compared to the stationary model. However, the model with the temperature covariate shows the smallest TIC, compared with the model including NAO and both.

### 3.2.3 | Statistical model evaluation

We combine the spatial dependence ( $Z$  series) and the marginal distribution models by Equation (13) and evaluate how well the statistical model performs:

$$W = \mu + \sigma \frac{Z^\xi - 1}{\xi} \quad (13)$$

We selected the same grid point  $s_0$  (Potsdam, 12.95 E, 52.95 N) and computed the extremal concurrent

**TABLE 5**  $\Delta$  values (%) of 20- and 50-year return levels of max-stable model in summer and winter; 5 and 95% confidence intervals shown in brackets

	Summer	Winter
20-year	10.53 (8.97, 12.09)	9.85 (7.69, 12.01)
50-year	14.77 (11.26, 18.28)	12.61 (9.73, 15.49)

coefficient ( $p$ ) over all pairs of grid points ( $s_0, s$ ) in the max-stable model (Figure 8). Even though the max-stable model shows an overestimated range of high dependence in the northern and southern regions of the selected grid, especially in winter, the dependence pattern is closer to the observations compared with most RCMs. The mean values of  $p$  are .34 and .36, respectively (Table 2). Our model is also able to represent the west–east asymmetric decay of the spatial dependence. That is consistent with observations in that the western regions to  $s_0$  are more dependent on the extremes at the selected point. Compared with the RCMs, the statistical model presents a more reliable spatial dependence of extremes.

The spatial distributions of the 20- and 50-year return periods between the max-stable model and E-OBS are shown in Figures 9 and 10. In summer, in the distribution of 20-year return levels, the large values in the north-eastern and southern part are underestimated by the max-stable model. While the distribution of intensities at 50-year return level shows that the max-stable

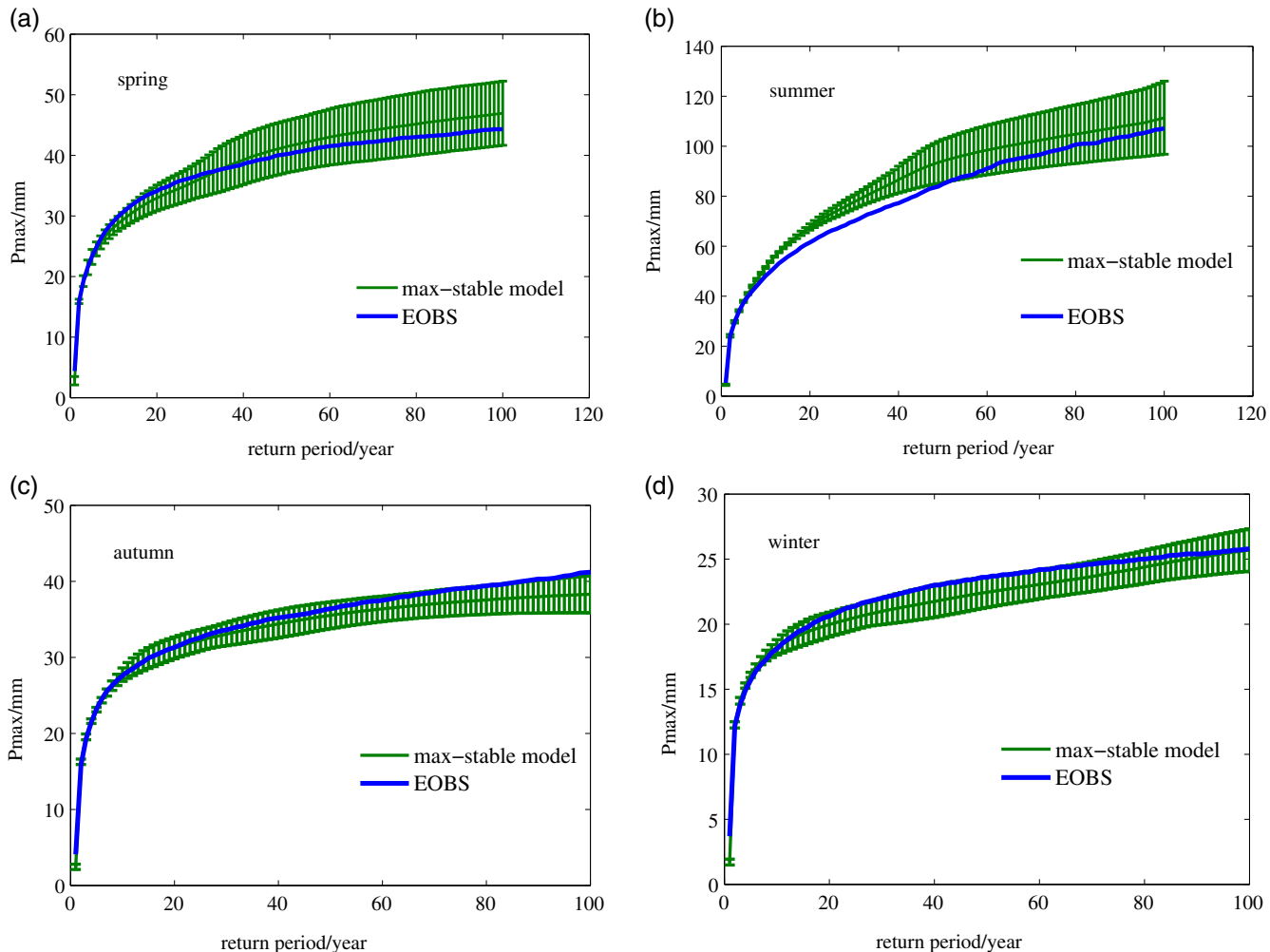


**FIGURE 11** Return period plots of extreme precipitation in (a) spring (b) summer (c) autumn (d) winter season of EOBS and the fitted max-stable model. The quantiles are calculated by aggregating over all grid points [Colour figure can be viewed at [wileyonlinelibrary.com](http://wileyonlinelibrary.com)]

model overestimates the south-eastern part. In general, the max-stable model is able to show the small values in the north-west, large values in the south-east, similar to E-OBS. The magnitudes at most grid points are well estimated. In winter, in the distributions of 20-year and 50-year return levels, the statistical model underestimates some extremes in the south-western part. Overall, the max-stable model can well represent the spatial characteristics of extreme precipitation intensities. We also use  $\Delta$  (Equation (9)) to quantify the difference between the max-stable model and observation in Table 5. Compared with the RCMs, the statistical model shows a smaller deviation of extreme intensities, except for CERFACS-CCLM4 and MPI-CCLM4 in winter. The deviations of the two return levels are less than 15%. In the 50-year return level in summer, the  $\Delta$  values of the max-stable model are smaller than of any RCM analysed.

The magnitudes of extreme precipitation of other return levels in each season are also simulated quite well by the statistical model. Figure 11 shows the empirical plot of the extreme intensity and error bars at different return levels. The max-stable model shows an overestimation of magnitudes when the return periods is shorter than 50 years in summer. But for other seasons and for the return periods longer than 50 years in summer, the intensities simulated by the max-stable model are good and the E-OBS results are inside the 95% confidence bounds.

To sum up, the max-stable model is able to reproduce the spatial differences over the region and accurately estimates the magnitudes of the extremes. But there is still some detailed information that the statistical model cannot reproduce. Compared to the RCMs, we provide evidence that the statistical model can better present extreme precipitation. And one major advantage of our statistical model is the low computational expense, especially for high-resolution simulations.

## 4 | CONCLUSIONS

We evaluated RCMs and statistical models in simulating extreme precipitation regarding spatial dependence and intensities over the Brandenburg-Berlin region in Germany. Since RCMs are widely used as inputs for hydrological models, such as flood or river run-off models and climate change studies, the ability of accurately modelling spatial extreme precipitation is needed. Our results show that none of the RCMs can reproduce well the spatial dependence of extreme precipitation. For instance, the RCMs have problems to accurately simulate how extremes of surrounding areas are dependent on the

occurrence of an extreme event at a specific single location. The area to the west of the selected grid point is more likely to be influenced than the east. But none of the RCMs can reproduce this east-west asymmetry. This asymmetry might be caused by large-scale precipitation systems which predominantly come from the west. However, more research is needed to better understand this phenomenon.

Among the five RCMs, the probability distribution of the extremal coefficient of MPI-CCLM4 does not change with distance in all seasons, which indicates that MPI-CCLM4 lacks the ability to characterize the spatial structures of extreme precipitation. In summer, the spatial dependences of CERFACS-CCLM4 are significantly underestimated. Other RCMs can roughly reproduce the observational patterns. In the aspect of intensity, most of the RCMs significantly underestimate the magnitude in summer and overestimate it in autumn and winter.

Compared with RCMs, the statistical max-stable model provides a much more efficient way in modelling precipitation extremes. It can reproduce the east-west asymmetry of spatial dependence and better reproduce geographical distributions and intensities of extremes than the RCMs. In modelling the marginal distribution of extremes, we find that in winter, the statistical model including the temperature covariate is the best, which means the extreme precipitation intensities are significantly associated with temperature in winter over this region (Scherrer and Baettig, 2008). The finding is consistent with previous studies in which the increase of heavy extreme precipitation has been attributed to global warming (Trenberth *et al.*, 2003; Shiu *et al.*, 2012). Here we predict that the extreme precipitation intensity may be heavier due to the global warming in the future. We could potentially produce statistical future projections by using projected temperatures from regional climate simulations as a covariate. It is a potential application of statistical models which still needs further study.

## ACKNOWLEDGEMENTS

CF was supported by the Collaborative Research Center TRR 181 ‘Energy Transfer in Atmosphere and Ocean’, funded by the Deutsche Forschungsgemeinschaft (DFG, German Research Foundation)—Projektnummer 274762653. ZT was supported by National Natural Science Foundation of China (Grant No. 41675049). We wish to thank Dr. Mathieu Ribatet for providing the ‘SpatialExtremes’ R package.

## ORCID

Lichao Yang  <https://orcid.org/0000-0001-5124-3406>

## REFERENCES

- Bárdossy, A. and Pegram, G. (2009) Copula based multisite model for daily precipitation simulation. *Hydrology and Earth System Sciences*, 13(12), 2299–2314.
- Bárdossy, A. and Pegram, G. (2012) Multiscale spatial re-correlation of RCM precipitation to produce unbiased climate change scenarios over large areas and small. *Water Resources Research*, 48 (9), W09502.
- Bell, J.L., Sloan, L.C. and Snyder, M.A. (2004) Regional changes in extreme climatic events: a future climate scenario. *Journal of Climate*, 17(1), 81–87.
- Berg, P., Christensen, O.B., Klehmet, K., Lenderink, G., Olsson, J., Teichmann, C. and Yang, W. (2019) Summertime precipitation extremes in a EURO-CORDEX 0.11 degrees ensemble at an hourly resolution. *Natural Hazards and Earth System Sciences*, 19(4), 957–971.
- Brown, B.M. and Resnick, S.I. (1977) Extreme values of independent stochastic processes. *Journal of Applied Probability*, 14(4), 732–739.
- Burnham, K.P. and Anderson, D.R. (2002) Model selection and multi-model inference: a practical information-theoretic approach. *Technometrics*, 45(2), 181.
- Cabral, R., Ferreira, A. and Friederichs, P. (2019) Space-time trends and dependence of precipitation extremes in North-Western Germany. *Environmetrics*, 31(3), e2605.
- Caroletti, G.N., Coscarelli, R. and Caloiero, T. (2019) Validation of satellite, reanalysis and rcm data of monthly rainfall in Calabria (Southern Italy). *Remote Sensing*, 11(13), 1625.
- Casanueva Vicente, A., Rodríguez Puebla, C., Frías Domínguez, M. D. and González Reviriego, N. (2014) Variability of extreme precipitation over Europe and its relationships with teleconnection patterns. *Hydrology and Earth System Sciences*, 18, 709–725.
- Casson, E. and Coles, S. (1999) Spatial regression models for extremes. *Extremes*, 1(4), 449–468.
- Chen, C.-T. and Knutson, T. (2008) On the verification and comparison of extreme rainfall indices from climate models. *Journal of Climate*, 21(7), 1605–1621.
- Christensen, J.H., Kjellström, E., Giorgi, F., Lenderink, G. and Rummukainen, M. (2010) Weight assignment in regional climate models. *Climate Research*, 44(2–3), 179–194.
- Coles, S., Bawa, J., Trenner, L. and Dorazio, P. (2001) *An Introduction to Statistical Modeling of Extreme Values*. Springer, London.
- Cooley, D., Naveau, P. and Poncet, P. (2006) Variograms for spatial max-stable random fields. In: *Dependence in Probability and Statistics*. Springer, New York.
- Cooley, D., Nychka, D. and Naveau, P. (2007) Bayesian spatial modeling of extreme precipitation return levels. *Journal of the American Statistical Association*, 102(479), 824–840.
- Cooley, D. and Sain, S.R. (2010) Spatial hierarchical modeling of precipitation extremes from a regional climate model. *Journal of Agricultural, Biological, and Environmental Statistics*, 15(3), 381–402.
- Davison, A.C. and Gholamrezaee, M.M. (2011) Geostatistics of extremes. *Proceedings of the Royal Society A: Mathematical, Physical and Engineering Sciences*, 468(2138), 581–608.
- Davison, A.C., Padoan, S.A. and Ribatet, M. (2012) Statistical modeling of spatial extremes. *Statistical Science*, 27(2), 161–186.
- De Haan, L. (1984) A spectral representation for max-stable processes. *The Annals of Probability*, 12(4), 1194–1204.
- De Haan, L. and Pereira, T.T. (2006) Spatial extremes: models for the stationary case. *The Annals of Statistics*, 34(1), 146–168.
- Dombry, C., Ribatet, M. and Stoev, S. (2018) Probabilities of concurrent extremes. *Journal of the American Statistical Association*, 113(524), 1565–1582.
- Dyrrdal, A.V., Stordal, F. and Lussana, C. (2018) Evaluation of summer precipitation from EURO-CORDEX fine-scale RCM simulations over Norway. *International Journal of Climatology*, 38 (4), 1661–1677.
- Ehmele, F., Kautz, L.-A., Feldmann, H. and Pinto, J.G. (2019) Long-term variances of heavy precipitation across Central Europe using a large ensemble of regional climate model simulations. *Earth System Dynamics Discussions*, 47, 1.
- Frei, C., Christensen, J.H., Déqué, M., Jacob, D., Jones, R.G. and Vidale, P.L. (2003) Daily precipitation statistics in regional climate models: evaluation and intercomparison for the European Alps. *Journal of Geophysical Research: Atmospheres*, 108(D3), 4124.
- Gerstner, E.-M. and Heinemann, G. (2008) Real-time areal precipitation determination from radar by means of statistical objective analysis. *Journal of Hydrology*, 352(3–4), 296–308.
- Hannachi, A. (2014) Intermittency, autoregression and censoring: a first-order AR model for daily precipitation. *Meteorological Applications*, 21(2), 384–397.
- Hofstra, N., Haylock, M., New, M., Jones, P. and Frei, C. (2008) Comparison of six methods for the interpolation of daily, European climate data. *Journal of Geophysical Research: Atmospheres*, 113(D21110), 1–19.
- Hofstra, N., New, M. and McSweeney, C. (2010) The influence of interpolation and station network density on the distributions and trends of climate variables in gridded daily data. *Climate Dynamics*, 35(5), 841–858.
- Holsten, A., Vetter, T., Vohland, K. and Krysanova, V. (2009) Impact of climate change on soil moisture dynamics in Brandenburg with a focus on nature conservation areas. *Ecological Modelling*, 220(17), 2076–2087.
- Jacob, D., Petersen, J., Eggert, B., Alias, A., Christensen, O.B., Bouwer, L.M., Braun, A., Colette, A., Déqué, M., Georgievski, G., Georgopoulou, E., Gobiet, A., Menut, L., Nikulin, G., Haensler, A., Hempelmann, N., Jones, C., Keuler, K., Kovats, S., Kröner, N., Kotlarski, S., Kriegsmann, A., Martin, E., van Meijgaard, E., Moseley, C., Pfeifer, S., Preuschmann, S., Radermacher, C., Radtke, K., Rechid, D., Rounsevell, M., Samuelsson, P., Somot, S., Soussana, J.F., Teichmann, C., Valentini, R., Vautard, R., Weber, B. and Yiou, P. (2014) EURO-CORDEX: new high-resolution climate change projections for European impact research. *Regional Environmental Change*, 14(2), 563–578.
- Jenkinson, A.F. (1955) The frequency distribution of the annual maximum (or minimum) values of meteorological elements. *Quarterly Journal of the Royal Meteorological Society*, 81(348), 158–171.
- Jones, P. and Reid, P. (2001) Assessing future changes in extreme precipitation over Britain using regional climate model integrations. *International Journal of Climatology*, 21(11), 1337–1356.
- Kabluchko, Z., Schlather, M. and De Haan, L. (2009) Stationary max-stable fields associated to negative definite functions. *The Annals of Probability*, 37(5), 2042–2065.

- Moberg, A., Jones, P.D., Lister, D., Walther, A., Brunet, M., Jacobbeit, J., Alexander, L.V., Della-Marta, P.M., Luterbacher, J., Yiou, P., Chen, D., Klein Tank, A.M.G., Saladié, O., Sigró, J., Aguilar, E., Alexandersson, H., Almarza, C., Auer, I., Barriendos, M., Begert, M., Bergström, H., Böhm, R., Butler, C.J., Caesar, J., Drebs, A., Founda, D., Gerstengarbe, F.W., Micela, G., Maugeri, M., Österle, H., Pandzic, K., Petrakis, M., Srnec, L., Tolasz, R., Tuomenvirta, H., Werner, P.C., Linderholm, H., Philipp, A., Wanner, H. and Xoplaki, E. (2006) Indices for daily temperature and precipitation extremes in Europe analyzed for the period 1901–2000. *Journal of Geophysical Research: Atmospheres*, 111(D22106), 1–25.
- New, M., Todd, M., Hulme, M. and Jones, P. (2001) Precipitation measurements and trends in the twentieth century. *International Journal of Climatology*, 21(15), 1889–1922.
- Räisänen, J. and Joellsson, R. (2001) Changes in average and extreme precipitation in two regional climate model experiments. *Tellus A*, 53(5), 547–566.
- Renard, B. and Lang, M. (2007) Use of a Gaussian copula for multivariate extreme value analysis: some case studies in hydrology. *Advances in Water Resources*, 30(4), 897–912.
- Ribatet, M. (2009) *A user's Guide to the SpatialExtremes Package*. Lausanne, Switzerland: EPFL.
- Ribatet, M. (2017) Modelling spatial extremes using max-stable processes. In: *Modelling Spatial Extremes Using Max-Stable Processes*. In Nonlinear and Stochastic Climate Dynamics: Cambridge University Press.
- Rulfová, Z., Beranová, R. and Kysely, J. (2017) Climate change scenarios of convective and large-scale precipitation in The Czech Republic based on EURO-CORDEX data. *International Journal of Climatology*, 37(5), 2451–2465.
- Santos, J., Corte-Real, J., Ulbrich, U. and Palutikof, J. (2007) European winter precipitation extremes and large-scale circulation: a coupled model and its scenarios. *Theoretical and Applied Climatology*, 87(1–4), 85–102.
- Scherrer, S.C. (2011) Present-day interannual variability of surface climate in CMIP3 models and its relation to future warming. *International Journal of Climatology*, 31(10), 1518–1529.
- Scherrer, S.C. and Baettig, M.B. (2008) Changes and inter-model spread in 21st century scenarios for temperature and precipitation extremes as seen with the climate change index (CCI). *Environmental Research Letters*, 3(3), 034005.
- Scherrer, S.C., Begert, M., Croci-Maspoli, M. and Appenzeller, C. (2016) Long series of Swiss seasonal precipitation: regionalization, trends and influence of large-scale flow. *International Journal of Climatology*, 36(11), 3673–3689.
- Schlather, M. (2002) Models for stationary max-stable random fields. *Extremes*, 5(1), 33–44.
- Schoelzel, C. and Friederichs, P. (2008) Multivariate non-normally distributed random variables in climate research—introduction to the copula approach. *Nonlinear Processes in Geophysics*, 15(5), 761–772.
- Shiu, C.-J., Liu, S.C., Fu, C., Dai, A. and Sun, Y. (2012) How much do precipitation extremes change in a warming climate? *Geophysical Research Letters*, 39(17707), 1–5.
- Sunyer, M., Luchner, J., Onof, C., Madsen, H. and Arnbjerg-Nielsen, K. (2017) Assessing the importance of spatio-temporal rcm resolution when estimating sub-daily extreme precipitation under current and future climate conditions. *International Journal of Climatology*, 37(2), 688–705.
- Thibaud, E., Mutzner, R. and Davison, A.C. (2013) Threshold modeling of Climatology of extreme spatial rainfall. *Water Resources Research*, 49(8), 4633–4644.
- Trenberth, K.E., Dai, A., Rasmusson, R.M. and Parsons, D.B. (2003) The changing character of precipitation. *Bulletin of the American Meteorological Society*, 84(9), 1205–1218.
- Varin, C. and Vidoni, P. (2005) A note on composite likelihood inference and model selection. *Biometrika*, 92(3), 519–528.
- Westra, S. and Sisson, S.A. (2011) Detection of non-stationarity in precipitation extremes using a max-stable process model. *Journal of Hydrology*, 406(1–2), 119–128.
- Yang, L., Franzke, C.L. and Fu, Z. (2019) Power-law behaviour of hourly precipitation intensity and dry spell duration over the United States. *International Journal of Climatology*, 40(4), 2429–2444.

**How to cite this article:** Yang L, Franzke CLE, Fu Z. Evaluation of the ability of regional climate models and a statistical model to represent the spatial characteristics of extreme precipitation. *Int J Climatol*. 2020;1–17. <https://doi.org/10.1002/joc.6602>